Academic Journal of Science and Technology
ISSN: 2771-3032 | Vol. 14, No. 2, 2025

High-Frequency Water Level Study Based on Multi-System GNSS-IR

Aofei Wu*

College of Surveying, Mapping and Land Information Engineering, Henan Polytechnic University, 454003, China
*Correspondence: 212204020074@home.hpu.edu.cn

Abstract: Accurate and high-frequency sea level monitoring is crucial in oceanic and global climate studies, but traditional techniques have their limitations. Over the past few decades, the application of Global Navigation Satellite System Multipath Reflection (GNSS-MR) in sea level monitoring has rapidly developed. Recently, the availability of more GNSS signals is expected to bring new opportunities to enhance its performance and achieve high spatiotemporal resolution. To fully utilize short-term multipath oscillation information, we conducted a GNSS-IR experiment using observation data from the BRST station in the first half of September 2024. The sliding window method was applied to collect Signal-to-Noise Ratio (SNR) sequences, and indicators such as peak-to-noise ratio and kurtosis were used to select appropriate spectral results. This enabled high-frequency water level monitoring with a 5-minute interval, achieving a correlation coefficient of over 0.9 and accuracy at the decimeter level, validating the performance and application prospects of GNSS-IR for water level monitoring.

Keywords: GNSS-IR, sliding window, SNR, high-frequency.

1. Introduction

The Global Navigation Satellite System (GNSS) is the collective term for all global satellite navigation systems and regional augmentation systems, including the United States' Global Positioning System (GPS), Russia's GLONASS, China's BeiDou Navigation Satellite System (BDS), the European Union's Galileo Navigation Satellite System, as well as Japan's Quasi-Zenith Satellite System and India's regional navigation satellite systems. GNSS continuously transmits L-band signals, providing users with high-precision positioning, navigation, and timing information, making it widely applied in fields such as land surveying, transportation, and public safety. With the continuous expansion of GNSS applications, GNSS reflection signals can provide features of reflective surfaces and geophysical parameters. Specifically, GNSS reflection measurement technology, or traditional GNSS-R technology, is a method for inverting surrounding environmental parameters using reflected signals received by geodetic-type GNSS receivers. It has now been adopted as a new remote sensing technique used for measuring sea surface height, soil moisture, snow depth, and other parameters.

Water level information is critical in hydrology, meteorology, and other important fundamental data, and its accurate real-time monitoring is vital for the safety of people's lives and property, as well as national social stability. GNSS-R technology offers a new approach for water level monitoring. The origin of GNSS-IR (Global Navigation Satellite System - Interferometric Reflectometry) technology can be traced back to the 1990s. In 1988, the European Space Agency (ESA) first proposed that GPS L-band signals could be used as scatterometers for ocean remote sensing research. Since then, researchers have gradually started using GNSS-R for sea surface height measurements (Hall et al., 1998). In 1993, European Space Agency scientist Martin-Neira introduced the PARIS (Passive Reflectometry and Interferometry System) concept, combining GPS direct and reflected signals to construct models for estimating sea surface height (Martin et al., 1993). GNSS-IR can mainly be implemented using signal-to-noise ratio (SNR) methods and carrier phase methods, with the SNR method being more widely studied. Additionally, the SNR method typically includes single-antenna and dual-antenna modes, depending on the number of antennas. The single-antenna mode is the most common GNSS-IR configuration, usually requiring only one antenna to receive reflected signals, which has advantages such as simple equipment, low cost, and strong adaptability, making it suitable for monitoring static or dynamic environments.

Anderson from the University of Colorado (Anderson, 2000) applied the principle and method of measuring the height from the GPS antenna phase center to the water surface. Based on the theory that signals in low elevation angle ranges from the water surface reflection interfere with the original signals, SNR observations were used to establish an interference model for calculating sea surface height. In 2004, Bilich and others separated the GPS receiver's SNR observations into direct and reflected signals and explored the mapping relationship between the characteristics of reflected signals and surrounding reflection surfaces, considering the impact of multipath effects in the station's environment (Bilich et al., 1992). Over the next few years, Larson and others systematically described the GNSS-IR SNR method and successfully applied it to monitor surface parameters such as tidal levels, vegetation, soil moisture, snow depth, and more (Larson et al., 2017; Larson et al., 2013; Larson, 2016), which played an important guiding role in subsequent scientific research. Its application was further extended to research areas such as permafrost, storm surges, and urban modeling (Lin et al., 2018; Peng et al., 2019; Ye et al., 2024). In 2013, Larson and others conducted SNR-based water level inversion experiments at two coastal stations using a single large measurement GPS receiver. Compared to the local nearby tidal station's measured data, the final correlation coefficient exceeded 0.97, and the root mean square (RMS) error was less than 5 cm and 10 cm, respectively (Larson et al., 2013; Larson et al., 2013; Löfgren et al., 2011). Löfgren (2014) used GPS and GLONASS signals for sea level height

measurement experiments, evaluating both SNR analysis and phase delay analysis methods. Their research showed that SNR analysis performs better in rougher sea conditions, especially when wind speeds reach 17.5m/s, whereas phase delay analysis becomes difficult when wind speeds exceed 6m/s. This demonstrated that GNSS-IR can maintain high accuracy for water level inversion while being more resilient to strong winds, making it a potential alternative to conventional tide gauges. Jin (Jin et al., 2011; Jin et al., 2011; Jin et al., 2017) first used BeiDou signals across three frequency bands (B1, B2, B3) for water level inversion using SNR data, and the experimental results showed a high correlation between the SNR method and phase method in measuring sea level changes. Purnell and others (Purnell et al., 2021) conducted tidal monitoring experiments using more low-cost antennas for GNSS-IR, with RMSE values ranging from 0.7 to 1.2 cm, significantly improving the inversion accuracy compared to single-antenna results. In 2023, Altuntas et al. (2023) proposed an empirical method to determine the optimal azimuth and satellite elevation angle for GNSS-IR water level inversion. After determining the best angles during a pre-analysis period, the six-month SNR data inversion results had a daily estimation correlation exceeding 97%, and the RMSE was below 3.2 cm, indicating that the method effectively identifies the optimal azimuth and satellite elevation angle ranges.

2. Data Processing

2.1. Data sources

To evaluate the performance of the sliding window weighted combination of GNSS-IR for monitoring high-dynamic sea tides, this study selected the BRST station of the multi-GNSS experiment (MGEX) project located at the Penfeld River estuary in Brest, France, as the experimental station. The open-source observation data from September 1 to September 14, 2024 (day of the year 245 to 259) were downloaded for the sea level inversion experiment. MGEX, established by the International GNSS Service (IGS), is an international project that tracks, organizes, and analyzes all available GNSS signals from multiple stations worldwide. The BRST station is equipped with a TRIMBLE ALLOY receiver and a TRM57971.00 antenna, with a data frequency of 1 Hz. It can receive satellites from the GPS, GLONASS, GALILEO, and BDS systems, but 30 Hz observation data were used in this paper. The station is located only 292 meters away from the Brest tidal station, and the sea level height recorded at the tidal station can be accessed in the data documentation uploaded to the French tidal observation reference website.

Regarding the selection of signal frequencies, an experimental analysis in the literature (Wang et al., 2018) examined the inversion performance of each frequency point in the four major GNSS systems and validated the accuracy of single-signal GNSS-IR. Within the GPS L2 frequency band, S2X has a clear advantage over S2W. The Galileo system's S1X, S5X, and S7X showed relatively better performance. The precision of S1C and S2C in the GLONASS system is similar to that of S1P and S2P. The signal frequency points finally selected in this study are shown in Table 1.

The surrounding environment of the BRST station, as illustrated in Figure 1, shows a reflection height of 18 meters, with elevation angles of 5° and 10° corresponding to the first Fresnel reflection zone. From Figure 1, it can be observed that the azimuth angle $\delta \in (180^\circ, 330^\circ)$ corresponds to the relatively narrow Penfeld River channel, hence the elevation angle is restricted to $\varepsilon \in (10^\circ, 30^\circ)$. Meanwhile, the azimuth angle $\delta \in (130^\circ, 180^\circ)$ corresponds to the open sea area, so the elevation angle is restricted to $\varepsilon \in (7^\circ, 30^\circ)$.

After the selection based on these elevation and azimuth angle settings, the sky plots of the satellite trajectories for GPS, GLONASS, GALILEO, and BeiDou systems during the experimental period were drawn (as shown in Figure 2). It can be seen that different systems provided sufficiently large numbers of satellites with good continuity.

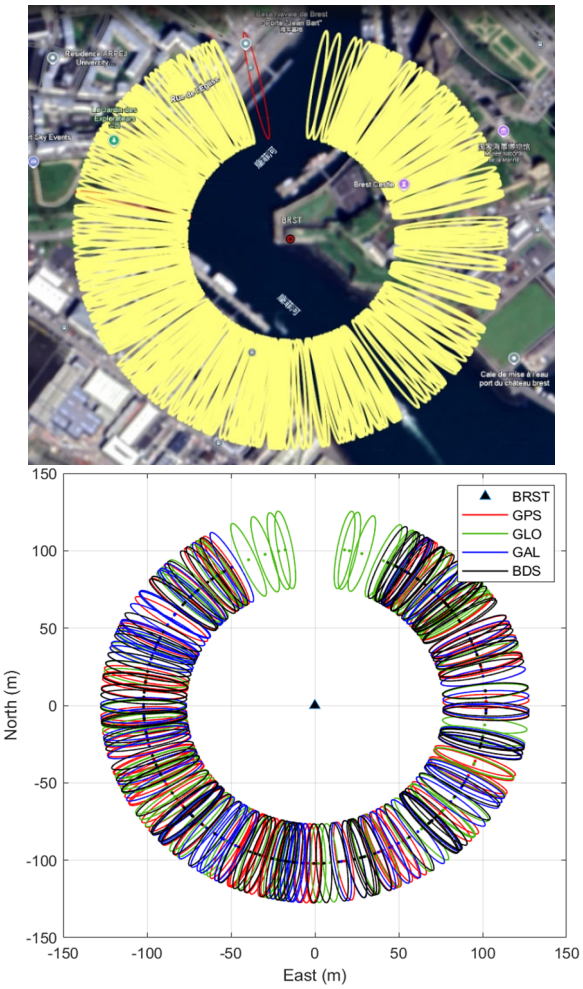

Figure 1. The first Fresnel zone at a reflection height of 18m at the BRST station (elevation angles of 5° and 10°).

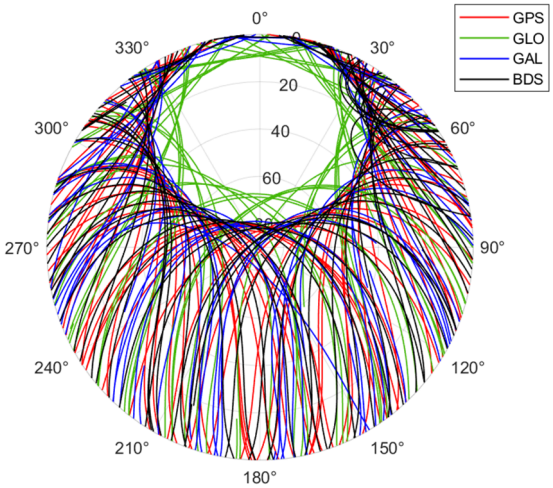

Figure 2. GNSS Satellite Sky Plot.

Table 1. GNSS signal frequency band and observation type used in BRST station experiment

satellite system	Signal frequency band	Signal frequency / Hz	SNR observations
GPS	L1	1575.420	S1C
	L2	1227.600	S2X
	L5	1176.450	S5X
GLONASS	G1	1602+k*9/16 (k= -7 … +12)	S1C
	G2	1246+k*7/16	S2C
GALILEO	E1	1575.420	S1X
	E5a	1176.450	S5X
	E5b	1176.450	S7X
BDS	B1-2	1561.098	S2I
	B3	1268.520	S6I
	B2b	1207.140	S7I

2.2. The principle and method of GNSS-IR inversion of water level

The GNSS signal is essentially an electromagnetic wave, and the process of obtaining satellite services by the user is, in fact, the reception of electromagnetic wave signals transmitted by the satellites. Specifically, for GNSS systems, the signals transmitted by satellites are right-hand circularly polarized (RHCP), which means that the oscillation direction of the electric field rotates in a clockwise direction over time. By decomposing the circularly polarized signal, the GNSS signal can be viewed as a combination of horizontal and vertical polarization components. This polarization characteristic has an important impact on the receiver's signal acquisition and decoding process, especially in complex electromagnetic environments, where the polarization type influences the signal's propagation path and reflection characteristics.

To optimize the reception of signals from satellites, GNSS receivers are typically equipped with right-hand circularly polarized (RHCP) antennas, which enhance the reception of RHCP signals while suppressing left-hand circularly polarized (LHCP) signals. In the GNSS-IR water level inversion application, since the reflected signal typically exhibits left-hand circular polarization (LHCP) while the incident signal is right-hand circularly polarized (RHCP), to effectively capture the reflected signal and perform accurate water level inversion, it is usually necessary to choose observation data from low elevation angle intervals.

Multipath effect is one of the common sources of error in GNSS signal propagation, referring to the phenomenon where satellite signals, before reaching the receiver, propagate along multiple paths due to reflections or refractions from the ground, buildings, water bodies, or other objects. These multipath signals, when combined with the direct signal, cause biases in pseudorange, carrier phase, and signal-to-noise ratio (SNR) measurements, thereby affecting GNSS positioning and measurement accuracy. Figure 3 illustrates the geometric model of GNSS multipath interference effects when the water surface is used as the reflection surface. The height of the receiver phase center relative to the reflection surface (in this case, the water surface) is denoted as H, and the elevation angle of the satellite is θ. The geometric delay of the reflected signal relative to the direct signal can be expressed as:

$$D = D_1 + D_2 = 2H * sin\theta$$

The geometric delay will cause the phase difference ψ between the reflected signal and the direct signal. When the carrier wavelength is λ, it can be expressed as :

$$\psi = \frac{2\pi D}{\lambda} = \frac{4\pi H * sin\theta}{\lambda}$$

Therefore, the signal received by the final receiver will be the interference signal between the direct signal and the reflected signal, and the phenomenon of the deviation between the observed value and the true value is called ' multipath effect.

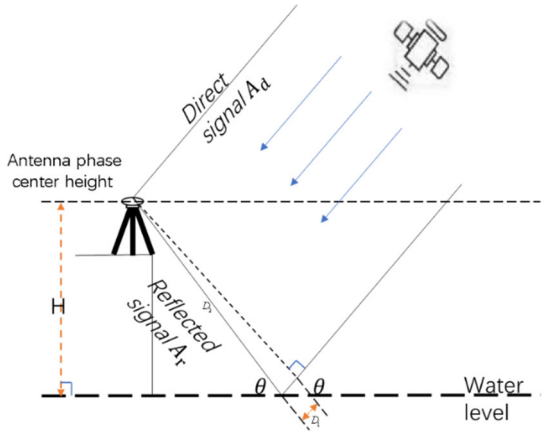

Figure 3. GNSS multipath interference geometric model

The observation file output by the GNSS receiver contains the signal-to-noise ratio (SNR) observations that measure the quality of the satellite signal. It is defined as the ratio of signal power P_R to noise power N, that is :

$$SNR = \frac{P_R}{N}$$

Signal-to-noise ratio (SNR) observations are usually measured in decibels (dB). The higher the value, the better the signal quality. The noise power is usually expressed by the thermal noise temperature T and the receiver front-end signal bandwidth B_w :

$$N = kTB_w$$

The unit of T is Kelvin (K), k is Boltzmann constant 1.38×10^{-23}, and the unit of B_w is Hertz (Hz). In practical applications, the signal-to-noise ratio provided in the GNSS observation file is actually the carrier-to-noise ratio C/N0. It is defined as :

$$\mathrm{C/N0} = \frac{P_R}{N_0}$$

Among them, N0 is the noise power spectral density. Compared with SNR, C/N0 eliminates the influence of bandwidth by normalizing the noise bandwidth, making it more suitable for the comparison of signals in different GNSS bands. From this, we can get:

$$\mathrm{C/N0} = SNR \cdot B_w$$

Therefore, the unit of C/N0 is usually dB Hz. The SNR data in the GNSS observation file used in this paper is the above carrier-to-noise ratio C/N0, but the SNR observation value is still written according to the habit. Because the SNR observation value in dB-HZ has a small response to the change of satellite elevation angle and a small fluctuation of amplitude fluctuation, it is generally linearized :

$$SNR_{\mathrm{volts/volts}} = 10^{SNR_{\mathrm{dB\cdot Hz}}/20}$$

When the GNSS receiver is placed at the edge of the water, due to the multipath effect, when some signals are reflected to the antenna through the water surface, the SNR observation

value will increase first and then decrease, accompanied by obvious periodic oscillation. The multipath effect can be exacerbated at low elevation angles, resulting in an oscillatory change in SNR (Pascual et al., 2014). Using this feature, the phase difference of the reflected signal can be inverted based on the SNR observations, and then the signal reflection height h can be inverted. SNR observations have the following relationship:

$$SNR^2 \approx A_c^2 = A_d^2 + A_r^2 + 2A_dA_r\cos\psi$$

The SNR observation value is a function of the direct signal amplitude A_d, the multipath reflection signal amplitude A_r and the phase difference ψ between the two. A_c and ψ_0 represent the amplitude and phase of the interference signal after the superposition of the direct signal and the reflected signal, as shown in Figure 4.

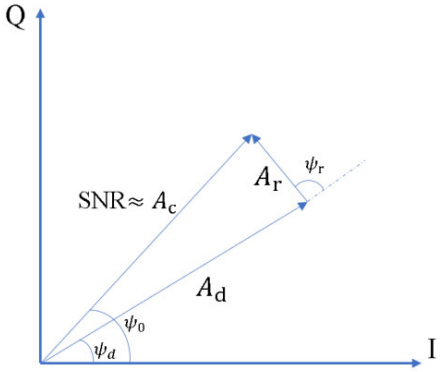

Figure 4. The interference superposition process of direct signal and reflected signal of GNSS

As mentioned above, the antenna of the measurement receiver is designed to be right-handed circularly polarized, so that more right-handed circularly polarized direct signals are received, and the left-handed circularly polarized reflected signals under the multipath effect are suppressed, thereby $A_d \gg A_r$. The direct signal in SNR is fitted by establishing a model, and then the SNR residual sequence containing the reflected signal information is obtained by removing the trend term. Common methods include low-order polynomials, empirical mode decomposition (EMD), and variational mode decomposition (VMD). Combining $\psi = \frac{2\pi D}{\lambda} = \frac{4\pi H * sin\theta}{\lambda}$ and $SNR^2 \approx A_c^2 = A_d^2 + A_r^2 + 2A_dA_r\cos\psi$, the residual sequence of low elevation angle can be expressed as

$$dSNR = A\cos\left(\frac{4\pi h}{\lambda}\sin\theta + \psi_0\right)$$

Suppose $t = \sin\theta$, $f = \frac{2h}{\lambda}$, then:

$$dSNR = A\cos(2\pi ft + \psi_0)$$

The SNR residual sequence after removing the trend term is a standard version of the cosine function expression. Because the oscillation frequency f contains the parameter, we can obtain the vertical height h from the antenna to the water surface by solving the oscillation frequency f:

$$h = \frac{\lambda f}{2}$$

Because sinθ is non-equidistant sampling, the Lomb-Scargle Fourier transform method can effectively analyze the time-domain non-uniform dSNR sequence, so as to extract the oscillation frequency f, so as to realize the inversion of water level parameters. One of the advantages of SNR altimetry is that the inversion of water level height can be realized by using single antenna and common geodetic measurement receiver without changing the structure of receiver and antenna.

2.3. Data processing

The observation files obtained by the GNSS receiver include SNR observations and carrier phase observations at each frequency point. First, the corresponding navigation ephemeris files need to be downloaded. Then, the single point positioning of the receiver is carried out, and the altitude angle and direction angle of each satellite in each observation epoch are calculated. The SNR at low elevation angle mentioned above will fluctuate violently due to the intensification of multipath effect, so the SN data is clipped according to the selected azimuth and low elevation angle range.

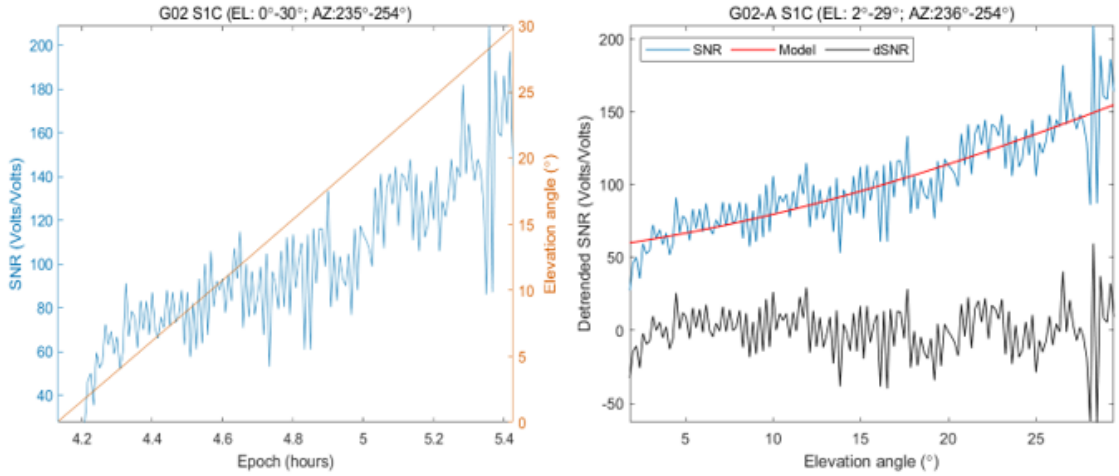

Figure 5. DOY244 G02 S1C signal

Figure 5 shows the SNR time series of the S1C signal from satellite G02 on DOY 244. It can be seen that the SNR fluctuates significantly at low elevation angles. The subsequent figure shows the residual sequence of SNR for the entire segment after fitting the direct signal with a quadratic polynomial model, removing the trend term.

In existing studies, researchers typically first calculate the reflected elevation (denoted as RH) estimates obtained from

the visible satellite arcs, and then apply a sliding window to the time series of estimates. For example, Roussel et al. (2015) used this method to analyze the performance of the sliding time window. In this experiment, the time resolution is 5 minutes, and the window width is 60 minutes. To avoid the shortcomings of the above method, this paper directly clips the time series of observation values, elevation angles, and azimuth angles after they are generated. Observation sequences with a window length of less than 300 seconds are removed.

The clipped observation sequence is then rearranged in ascending order of elevation angle and fitted using a low-order polynomial, with the trend term being removed. The main frequency is extracted using the L-S periodogram (Lomb et al., 1976; Scargle et al., 1982). If the observation is an SNR value, it can be directly multiplied by λ/2 to estimate the static reflected elevation RH. To prevent outliers, the maximum and minimum limits of the main frequency need to be restricted according to the actual environment of the station. Additionally, to avoid unclear spectral peaks, a threshold for the main frequency amplitude is set, and the Peak to Noise Ratio (PNR) parameter is defined as follows:

$$PNR = \frac{A_p}{\sum_{i=1}^{N} A_i / N}$$

Where A_p p is the maximum amplitude in the frequency domain, A_i is the amplitude of the i th frequency point in the frequency domain, and N is the total number of frequency points of the discrete frequency sequence converted from the L-S periodic diagram. This parameter is used to represent the significance of the dominant frequency peak of the frequency sequence, and its lower limit is usually set to 3.

After obtaining the inversion results of all windows, in order to prevent the influence of gross errors on the subsequent least squares estimation, and to facilitate the subsequent comparison of the performance of different systems and signal frequency points, this paper removes outliers from all estimates in each window. First, the interquartile range (IQR) of all estimates is calculated, that is, the difference between the third quartile Q3 and the first quartile Q1 :

$$IQR = Q3 - Q1$$

And set the outlier range as follows :

$$x = \{x | x \leq Q1 - 1.5 * IQR \vee x \geq Q3 + 1.5 * IQR\}$$

In order to make full use of the prior conditions, this paper uses a quality index called local kurtosis (LK) to set the weight value. The LK of the L-S periodogram is defined as the kurtosis of the sequence of a specific number of frequency points (usually about 300 each) before and after the peak frequency point, which can represent the sharpness of the main frequency peak. The sharper the peak is, the greater the kurtosis is, indicating that the relative noise of the dominant frequency peak is more significant, and the higher the inversion quality is, the threshold can usually be set according to the specific situation. In order to find the most appropriate numerical weighting, the form of an exponential function can be used to adjust the discrimination of the weight to the dominant frequency significance :

$$P_i = \frac{\mu^{LK_i}}{\nu}$$

Where P_i is the weight of the i-th estimate, and LK_i is the local kurtosis of the i-th estimate. μ and ν are exponential adjustment factor and proportional adjustment factor, respectively. Generally, the optimal values of μ and ν can be found by prior data.

3. Analysis of Experimental Results

3.1. Analysis of Single Frequency Point Results

We inverted the data of each frequency point in the BRST station observation file, and compared the estimated value with the tidal station data of the Brest station. The results are shown in Fig.6. In addition, the statistics of the inversion results are shown in Table 2. More than half of the frequency points produce more than 200 observations per day. Among them, the RMSE of GLONASS-S1C is the smallest, while BDS-S6I provides the most observations. The RMSE of each frequency point is basically between 0.5 meters and 0.7 meters except BDS S7I.

When evaluating the performance of different SNR types, RMSE and the number of searches should be considered together. From the perspective of different systems, the GLONASS system has the highest accuracy, which can be seen from Figure 6 and Statistical Table 2. Figure 7 shows the correlation analysis between the estimated results of each frequency point and the measured values of the water level station. The correlation coefficient R^2 of the two frequency points of the GLONASS system is above 0.85, which is also the highest in the four systems. The performance of GPS system is second only to GLONASS.Although the correlation coefficient R^2 of the three frequency points of GPS is in the range of 0.71 to 0.85, the S5X observation value has a large RMSE, and the correlation coefficient of this frequency point is also the lowest among the three frequency points. It is speculated that there are a large number of outliers in the S5X estimation results of GPS that have not been effectively eliminated.

According to the analysis of the water level inversion results of the four satellite navigation systems (BeiDou, Glonass, GPS, Galileo) and their 11 frequency bands, the results show that there are significant differences in the performance of different systems and frequency bands in water level inversion. Firstly, the amount of data affects the inversion accuracy to a certain extent. The frequency bands with larger data volume, such as BeiDou's S6I band (2963 data points), show the best inversion effect, with RMSE of 0.605 m and R2 of 0.816, while the frequency bands with less data volume, such as BeiDou 's S7I band (330 data points), show larger inversion error, with RMSE of 0.922 m and R2 of only 0.385, showing lower correlation and larger fitting error. Similarly, Galileo 's S5X and S7X bands, despite the large amount of data, show lower errors and higher goodness of fit, while GPS 's S5X band shows relatively large RMSE and lower R2, reflecting the influence of different frequency bands on the inversion results.

In addition, signal quality and frequency band selection are key factors influencing inversion accuracy. The S1C frequency band of GLONASS performs the best, with an R^2 of 0.895 and an RMSE of 0.492 meters, likely due to the strong signal quality and satellite coverage of this band. In contrast, some frequency bands of GPS and BeiDou, such as GPS's S2X and S5X bands and BeiDou's S7I band, exhibit larger inversion errors and lower correlations due to weaker signal quality or multipath effects. The differences in inversion accuracy across different frequency bands are not only related to signal strength and quality but may also be closely linked to multipath effects, data processing methods, and satellite configurations. For example, although the S1X frequency band of Galileo has relatively fewer data points, its performance remains stable, likely due to its higher satellite

coverage and precise signal processing.

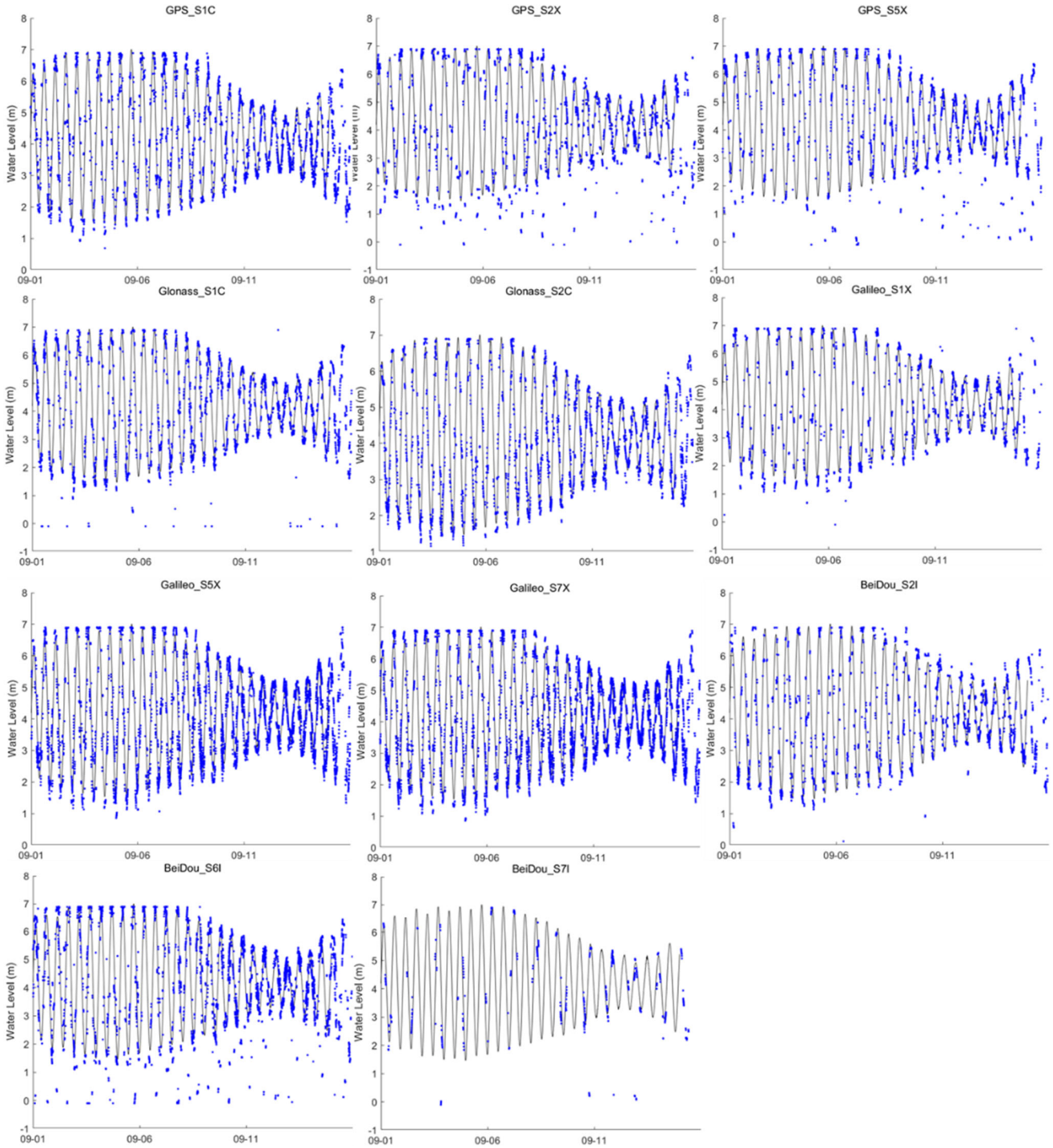

Figure 6. The inversion results of SNR observation type contained in BRST station observation file are shown.

Further analysis shows that the existing inversion algorithms and models exhibit differences in adaptability across frequency bands, especially for low-signal bands (e.g., S7I and S5X), where the algorithms may not be able to fully cope with signal noise or other environmental factors, leading to lower inversion accuracy. Therefore, optimizing existing inversion algorithms, particularly in processing methods for low-signal frequency bands, is crucial. Improving inversion accuracy for low-signal frequency bands may require combining multi-frequency data, employing data fusion techniques, and further improving noise suppression algorithms and error correction models. Overall, the performance ranking across systems is GLONASS>GPS> BeiDou > Galileo, which is consistent with previous studies (Tabibi et al., 2017; Zheng et al., 2021; Wang et al., 2019).

Table 2. Statistics of inversion results of SNR observation types contained in BRST station observation files

Observed type	Number	Average	RMSE(m)	R^2
BeiDou_S2I	1770	126	0.696	0.781
BeiDou_S6I	2963	212	0.605	0.816
BeiDou_S7I	330	24	0.922	0.385
Glonass_S1C	2716	194	0.492	0.895
Glonass_S2C	2872	205	0.529	0.856
GPS_S1C	2762	197	0.565	0.848
GPS_S2X	1910	136	0.679	0.762
GPS_S5X	1942	139	0.747	0.714
Galileo_S1X	1571	112	0.795	0.756
Galileo_S5X	3960	283	0.605	0.816
Galileo_S7X	4097	293	0.605	0.818

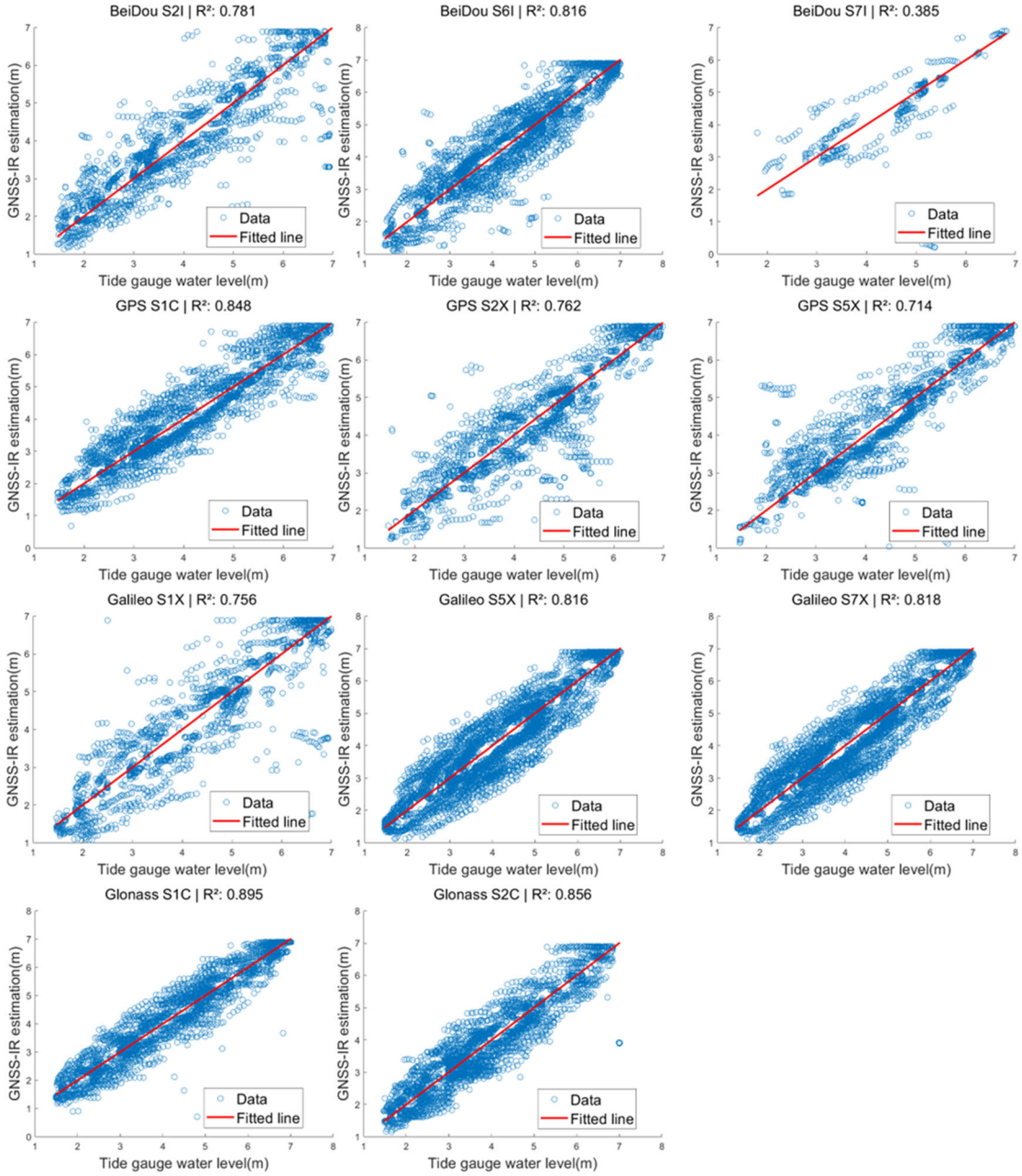

Figure 7. Correlation analysis of inversion results of each frequency point

The analysis shows that the amount of data and the choice of frequency band have a significant impact on the accuracy and fitting effect of water level inversion results. The S6I frequency band, with more data points and optimal inversion

accuracy and fitting effect, demonstrates strong superiority. In contrast, the S7I frequency band may be affected by insufficient data and an imperfect inversion model, requiring further optimization of the model and increased data samples to improve inversion accuracy. In conclusion, this study reveals the differences between various satellite systems and their frequency bands in water level inversion, particularly the impact of data volume, signal quality, and frequency band characteristics on inversion accuracy. For high-precision frequency bands (such as Glonass S1C and BeiDou S6I), inversion accuracy is better, but for low-signal frequency bands (such as BeiDou S7I and GPS S5X), inversion algorithms still need further optimization and data volume needs to be increased to enhance inversion accuracy. Future research can focus on data processing methods and algorithm optimization for low-signal frequency bands to improve overall inversion performance.

3.2. Multi-system inversion results

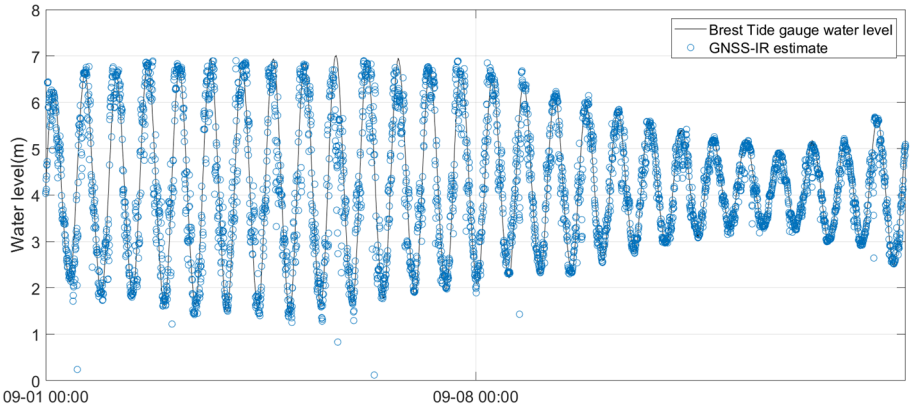

Figure 8. The estimation results of multi-frequency combined GNSS-IR by SNR method at BRST station.

Due to the 30-second sampling interval of the observation files, some sliding windows contain no SNR arc segments that meet the criteria, or due to a low SNR value, the fitting effect is poor, leading to the final multi-system combined result not strictly providing water level data at 5-minute intervals. To compensate for the missing estimates caused by observation interruptions or degraded observation quality, a smoothing interpolation method is attempted for repair. In previous studies on the GNSS-IR inverse model, some researchers used B-spline curves to simulate smoothly changing water levels (Strandberg et al., 2016), but this method has high parameter setting requirements and is not suitable for the current scenario. By using spline interpolation to achieve high-frequency water level inversion results with a 5-minute resolution, the overall correlation coefficient reaches 0.86, and the RMSE is reduced to around 0.5m. However, since there are a large number of invalid inversions in the single-frequency inversion results that were not effectively removed, the final multi-system results show only a small improvement compared to the single-system results.

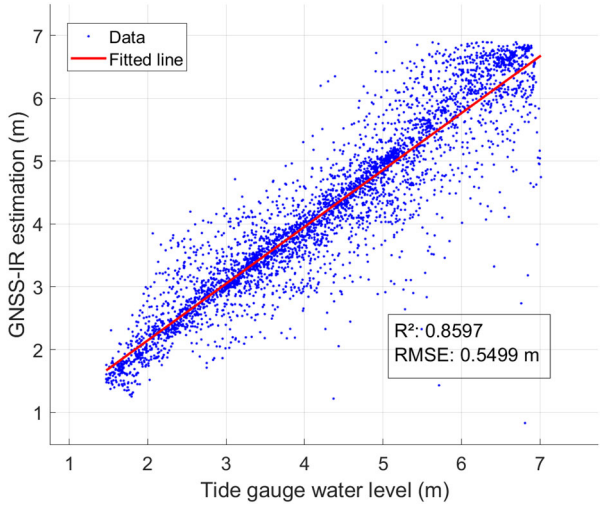

Figure 9. Correlation of estimation results of multi-frequency combined GNSS-IR based on SNR method at BRST station.

This chapter presents the inversion results based on SNR data for single-frequency GNSS-IR and multi-system integration. The model provides good accuracy in the water level results, ensuring a time resolution of 5-minute water level monitoring, with an RMSE of 0.5 meters. Compared to the traditional method of directly using SNR arc segments for inversion, this approach significantly improves the time resolution of GNSS estimates and successfully demonstrates a substantial enhancement in both the time resolution and inversion accuracy of the water level monitoring stations based on the original observational data. The experiment also concluded that the multi-frequency, multi-system model does not require corrections for frequency bands with biases in the inverted water levels. It integrates information from different frequency bands, providing better anti-interference capability than single-frequency inversion results.

4. Conclusion

This paper uses SNR observation data to explore the accuracy and stability of different system frequencies. The experimental results show that GLONASS has the highest accuracy among the four major systems, while GALILEO's results are generally poorer. GPS and BDS perform similarly in GNSS-IR, and because GNSS-IR only uses low-elevation satellites, the advantage in the number of BDS satellites is not significantly reflected. From the error analysis of two experimental groups, the larger errors in water surface height estimation are mainly distributed at the peaks and troughs of the water surface height change curve, with the specific reasons requiring further investigation.

References

[1] Hall C D, Cordey R A. Multistatic scatterometry[C]//International Geoscience and Remote Sensing Symposium, 'Remote Sensing: Moving Toward the 21st Century'. September 12-16, 1988, Edinburgh, UK. IEEE, 1988: 561-562.

[2] Martin-Neira M. A passive reflectometry and interferometry system (PARIS): Application to ocean altimetry[J]. ESA journal, 1993, 17(4): 331-355.

[3] Anderson K D. Determination of Water Level and Tides Using Interferometric Observations of GPS Signals[J]. Journal of Atmospheric & Oceanic Technology, 2000, 17(8): 1118-27.

[4] Bilich A, Larson K M, Axelrad P . Observations of signal-to-noise ratios (SNR) at geodetic GPS site CASA: Implications for phase multipath.

[5] Larson K M, Ray R D, Williams S D P . A 10-Year Comparison of Water Levels Measured with a Geodetic GPS Receiver Versus a Conventional Tide Gauge[J]. Journal of Atmospheric & Oceanic Technology, 2017, 34(2).

[6] Larson K M , Ray R D , Nievinski F G , et al. The Accidental Tide Gauge: A GPS Reflection Case Study From Kachemak Bay, Alaska[J]. IEEE Geoscience and Remote Sensing Letters, 2013, 10(5):1200-1204.

[7] Larson K M . GPS interferometric reflectometry: applications to surface soil moisture, snow depth, and vegetation water content in the western United States[J]. Wiley Interdisciplinary Reviews: Water, 2016, 3(6).

[8] Lin L , Larson K M . Decadal changes of surface elevation over permafrost area estimated using reflected GPS signals[J]. Cryosphere, 2018, 12(2):1-22.

[9] Peng D, Hill E M, Li L , et al. Application of GNSS interferometric reflectometry for detecting storm surges[J]. GPS Solutions, 2019, 23(2).

[10] Ye M, Zhang G, Hsu L T. Building Model Rectification Using GNSS Reflectometry[J]. IEEE Geoscience and Remote Sensing Letters, 2024.

[11] Larson K M, Ray R D, Nievinski F G, et al. The accidental tide gauge: a GPS reflection case study from kachemak bay, Alaska[J]. IEEE Geoscience and Remote Sensing Letters, 2013, 10(5): 1200-1204

[12] Larson K M, Loefgren J S, Haas R. Coastal Sea level measurements using a single geodetic GPS receiver[J]. Advances in Space Research, 2013, 51(8):1301-1310.

[13] Löfgren J S, Haas R, Scherneck H G, et al. Three months of local sea level derived from reflected GNSS signals[J]. Radio Science, 2011, 46(06): 1-12.

[14] LöFgren J S , Haas R . Sea level measurements using multi-frequency GPS and GLONASS observations[J]. Eurasip Journal on Advances in Signal Processing, 2014, 2014(1):1-13.

[15] Jin S G, Feng G P, Gleason S. Remote sensing using GNSS signals: Current status and future directions[J]. Advances in Space Research, 2011, 47(10):1645-1653.

[16] Jin S G, Cardellach E, Xie F. GNSS Remote Sensing：Theory, methods and applications [M]. Springer Netherlands, 2014.

[17] Jin S G, Qian X D, Wu X. Sea level change from BeiDou Navigation Satellite System-Reflectometry (BDS-R): First results and evaluation[J]. Global and Planetary Change, 2017, 149: 20-25.

[18] Purnell D J , Gomez N , Minarik W , et al. Precise water level measurements using low-cost GNSS antenna arrays[J]. Earth Surface Dynamics, 2021, 9(3):673-685.

[19] Altuntas C, Tunalioglu N. A systematic approach for identifying optimal azimuth and elevation angle masks in GNSS-IR: validation through a sea level experiment[J]. GPS Solutions, 2023, 27(4): 1-13.

[20] Pascual D, Park H, Camps A et al. Comparison of GPS L1 and Galileo E1 signals for GNSS-R ocean altimetry[C]// 2013 IEEE International Geoscience and Remote Sensing Symposium - IGARSS. IEEE, 2014.

[21] Montenbruck O, Steigenberger P, Prange L, et al. The Multi-GNSS Experiment (MGEX) of the International GNSS Service (IGS)–achievements, prospects and challenges[J]. Advances in space research, 2017, 59(7): 1671-1697.

[22] Wang X, Zhang Q, Zhang S. Azimuth selection for sea level measurements using geodetic GPS receivers[J]. Advances in Space Research, 2018, 61(6): 1546-1557. [J]. Advances in Space Research, 2018, 61(6): 1546-1557.

[23] Roussel N , Ramillien G , Frappart F , et al. Sea level monitoring and sea state estimate using a single geodetic receiver[J]. Remote Sensing of Environment, 2015.

[24] Lomb N R. Least-squares frequency analysis of unequally spaced data[J]. Astrophysics and space science, 1976, 39: 447-462.

[25] Scargle J D. Studies in astronomical time series analysis. II-Statistical aspects of spectral analysis of unevenly spaced data[J]. Astrophysical Journal, Part 1, vol. 263, Dec. 15, 1982, p. 835-853., 1982, 263: 835-853.

[26] S. Tabibi, F. Geremia-Nievinski, and T. van Dam, “Statistical comparison and combination of GPS, GLONASS, and multi-GNSS multipath reflectometry applied to snow depth retrieval,” IEEE Geosci. RemoteSens. Lett., vol. 55, no. 7, pp. 3773–3785, Jul. 2017.

[27] N. Zheng, P. Chen, and Z. Li, “Accuracy analysis of ground-based GNSS-R sea level monitoring based on multi GNSS and multi SNR,”Adv. Space Res., vol. 68, no. 4, pp. 1789–1801, Aug. 2021.

[28] X. Wang, X. He, and Q. Zhang, “Evaluation and combination of quadconstellation multi-GNSS multipath reflectometry applied to sea level retrieval,” Remote Sens. Environ., vol. 231, Sep. 2019, Art. no. 111229.

[29] Strandberg J, Hobiger T, Haas R. Improving GNSS-R sea level determination through inverse modeling of SNR data[J]. Radio science, 2016, 51(8): 1286-1296.